Catena 74 (2008) 165–174

Contents lists available at ScienceDirect

Catena

journal homepage: www.elsevier.com/locate/catena

Accounting for shape reliability in modeling contour-derived topographic properties for use in soil–terrain correlation

A. Sindayihebura [a,b,*], M. Van Meirvenne [a], S. Verstraete [a], S. Nsabimana [c]

[a] Department of Soil Management and Soil Care, Ghent University, Coupure 653, 9000 Gent, Belgium
[b] Department of Earth Sciences, University of Burundi, P.O. Box 1550 Bujumbura, Burundi
[c] Department of Geography, University of Burundi, P.O. Box 1550 Bujumbura, Burundi

ARTICLE INFO

Article history:
Received 15 October 2007
Received in revised form 17 April 2008
Accepted 22 April 2008

Keywords:
Digital elevation model
Interpolation
Simulation
Uncertainty

ABSTRACT

Elevation contours are known to be poor quality data for digital terrain modeling, but they are often the only available topographic information at national scale, especially in developing countries. We investigated several methods to derive elevation and slope data from contours for two contiguous watersheds in Burundi. Two key issues in digital terrain modeling were addressed: (1) finding the 'best' elevation interpolator, and (2) assessing the related uncertainty and its propagation to slope models. The key validation criterion was the reproduction of the terrain shape as inferred from the pattern of contours, which is more important than absolute accuracy in soil–terrain correlation. A method using a triangulated irregular network (TIN) and four grid-based methods were compared and combined. The most satisfactory results were achieved by combining the TIN-based method with a grid-based method. Treating contours as inequality constraints proved useful in simulating the elevation uncertainty. The Zevenbergen and Thorne and the Evans–Young slope algorithms were compared based on their sensitivity to the elevation uncertainty. Outputs from simulation were filtered to produce realistic alternative elevation models. In that case, the slope variance values were similar for the two algorithms, suggesting similar performances. Checking for shape reliability was found critical for the validation of topographic models.

1. Introduction

Contour lines of topographic maps are still the main source of topographic information, especially in developing countries. However, topography represents a continuous surface, and therefore these linear features have to be converted to a raster layer, known as a digital elevation model (DEM). Problems in interpolating a DEM from contours have been reported in literature (e.g. Burrough and McDonnell, 1998; Wilson and Gallant, 2000). They are related to the discrete distribution of elevation on a contour map. No information is provided in between consecutive contours, while only one elevation value is redundantly given along each contour trace. Therefore, more attention should be focused on contour-specific interpolators that properly approximate the terrain shape between contour lines. In this respect, the ideal contour-derived DEM or terrain shape is that inferred from visual interpretation of the pattern of contours. Most previous work has compared different DEM interpolators based only on global quantitative measures, such as the Root Mean Square Error (RMSE) (e.g., Kidner, 2003; Aguilar et al., 2005). However, in many applications, reproduction of the terrain shape is more important than absolute accuracy (Wise, 2000). Moreover, DEM errors are likely to vary spatially, but spatial variability cannot be described by global statistical measures (Fisher and Tate, 2006).

Qualitative criteria related to reproduction of the terrain shape inferred from contours have proved useful by, among others, Carrara et al. (1997) and Wise (2000), and have also been recommended in Wilson and Gallant (2000). For example, careful inspection of the original contours allows identification and approximate location of many landscape features (summits, pits, crests, river channels or ephemeral gullies, watershed boundary). The maximum uncertainty in the location of such features is typically equal to the contour interval for the *Z*-coordinate (elevation), and the distance between the surrounding contour(s) at map scale for the *X* and *Y* coordinates. However, unless an additional validation dataset is provided, the RMSE, and other quantitative measures, cannot help checking the reproduction of these features on interpolated DEMs.

The implicit and contour-derived information may be extended to assess the DEM uncertainty. Uncertainty assessment may be performed by analysis of discrepancies between numerous equally probable realizations produced using simulation methods (Goovaerts, 1997). For contour data, one needs to take into account that elevation values at points located between two contours are constrained by the two contour values. So far, assessing the uncertainty of DEMs by treating contour values as constraint intervals has not been tested.

* Corresponding author. Department of Soil Management and Soil Care, Ghent University, Coupure 653, 9000 Gent, Belgium.
E-mail address: anicet_fr@yahoo.fr (A. Sindayihebura).

0341-8162/$ – see front matter © 2008 Elsevier B.V. All rights reserved.
doi:10.1016/j.catena.2008.04.014

In many environmental applications, DEMs are used in combination with other topographic properties (e.g. slope gradient, slope aspect, slope curvature, upslope contributing area, and topographic wetness index) which are themselves derived from DEMs (e.g., Burrough and McDonnell, 1998; Shary et al., 2002). Therefore, DEM errors will propagate to the target variable (Heuvelink, 1998; Holmes et al., 2000; Biesemans et al., 2000). Sources of errors in DEMs are due to the quality of input data, the limitations of the algorithm used to model the topography and the complexity of the terrain (Wood, 1996). Consequently, for a given area where the elevation data are only contour lines, the only element under the control is the algorithm used. Many interpolation methods are available, but it is not clear to the user which interpolator is best for contour data. Special methods have been developed to account for the reproduction of the terrain shape (e.g. Hutchinson, 1996; Carrara et al., 1997; Jaakkola and Oksanen, 2000), but it seems no single method is satisfactory (Jaakkola and Oksanen, 2000). In this paper, several methods were investigated and combined, and preference was given to methods available in common GIS software.

The aim of this paper was to capitalize on the reproduction of terrain shape in generating DEMs and assessing DEM uncertainty and its effects on slope models. The main reasoning was that a correct DEM must portray the implicit geomorphologic characteristics (e.g. summits, pits, passes, crests, valleys) that can be inferred from explicit features of the original topographic maps (i.e. contour values and pattern, river channels). Special attention was paid to the choice of DEM resolution, which is prerequisite to DEM interpolation and limits the ability to portray geomorphologic characteristics. Notice that the contour values themselves are not error-free, but these errors are usually not documented. Therefore, we limited ourselves to topographic information readily available, i.e. contour data. The test site (14.8 km^2) was composed of two contiguous catchments in the Central Plateaus of Burundi which are characterized by a hilly landscape with round-shape summits, developed on folded Precambrian rocks. The research was conducted at a catchment scale so as to account for the landscape complexity at the catena level, i.e. from the valley floor to the hilltop or watershed divide. As such, the test site is a typical example of well differentiated landscapes that are abundant in the tropics.

2. Theory

2.1. Creating DEMs from contours

The first step toward creating a DEM from contour data is deciding on the minimum spacing between original elevation contours and the appropriate pixel size, also referred to as resolution or grid spacing, to be used in the DEM interpolation. A minimum spacing between sampling points must be determined to avoid spatial aliasing (Smith and Wessel, 1990; Carrara et al., 1997). Smith and Wessel (1990) consider that the minimum spacing between samples should be at least twice the grid spacing or resolution of the DEM. This requires prior knowledge about the appropriate resolution of the DEM that must be accounted for when digitizing or when cleaning the already digitized data. However, for some of the proposed approaches, finding the optimal resolution involves repeatedly creating DEMs using different resolutions, which becomes impractical. Examples of such methods were proposed in Hutchinson (1996) and Florinsky and Kuryakova (2000). For DEMs derived from contours, Hengl (2006) suggests three resolutions: (1) the coarsest resolution that should be equal to half the average spacing between contours, (2) the finest resolution that is given by the shortest spacing between contours, and (3) the compromise resolution that he defined as the 5-% probability distance between contours. An alternative method is the application of cartographic rules, stating that the optimal DEM resolution is equal to the maximum graphic resolution of lines shown on a map, i.e. 0.4 mm at map scale (Tempfli, 1999). Deciding on the appropriate DEM resolution is crucial since it controls the spatial detail, yet in many instances, the DEM resolution is chosen arbitrary or based on external motivations.

The next step is selecting the appropriate DEM interpolation method. Many researchers have focused on comparing DEM algorithms using global statistical indices, like the Mean Error (ME) and the Root Mean Square Error (RMSE). These indices are computed using interpolated values, $z^*(\mathbf{u}_\alpha)$, and reference values, $z(\mathbf{u}_\alpha)$ for n reference points (also known as validation points) ($\mathbf{u}_\alpha$) ($\alpha = 1, 2\ldots n$).

$$\mathrm{ME} = \frac{1}{n}\sum_{\alpha=1}^{n}\left[z^*(\mathbf{u}_\alpha) - z(\mathbf{u}_\alpha)\right] \tag{1}$$

$$\mathrm{RMSE} = \sqrt{\frac{\sum_{\alpha=1}^{n}\left[z^*(\mathbf{u}_\alpha) - z(\mathbf{u}_\alpha)\right]^2}{n}} \tag{2}$$

The ME represents the bias, whereas the RMSE measures the accuracy for a given interpolation method. Indices (1) and (2) can be combined to provide a measure of the precision of the interpolation method:

$$\mathrm{Precision} = \sqrt{\mathrm{RMSE}^2 - \mathrm{ME}^2} \tag{3}$$

According to Desmet (1997), the choice of an appropriate interpolation method is a compromise between precision and shape reliability. The following artifacts can be expected to exist in DEMs created with inappropriate interpolation methods or options:

(1) Over-shoots and under-shoots, that is, extrapolations to non-allowable maximum or minimum elevations. The difference in elevation between an interpolation point and the closest contour cannot be larger than the contour interval.
(2) Artificial terraces along contour traces. These are likely to occur for interpolators using too small search neighborhoods (Burrough and McDonnell, 1998; Jones, 1998).
(3) Tabular-shaped valleys, crests and summits passing to the closest contour trace. This is typical to interpolation methods that cannot extrapolate beyond the local contour range, like Moving Average and Inverse Distance Weighting.

All three types of artifacts are easily identified using common GIS operations. The first artifact may be identified by deriving contours with the same contour interval as that of the original contours. Overlay of the two contour maps will show over-shoots and under-shoots as new local contour maxima and minima, respectively. The last two types of artifacts correspond to the case where all the eight pixels around the central pixel in a three by three pixel window receive an identical value (Hengl et al., 2003). Local minima and maxima are often under-represented on topographic maps by too few elevation points in valleys and at summits. Surprisingly, interpolation methods that cannot extrapolate beyond the data range are still used in DEM interpolations.

2.2. Modeling uncertainty for contour-derived DEMs

Most studies on DEM uncertainty focused on deriving uncertainty for a specific DEM. This required the use of validation data to compute the error and model its spatial variability, then simulate it and finally add it to the DEM (Fisher, 1998; Holmes et al., 2000; Raaflaub and Collins, 2006). Even without extra data the DEM uncertainty can be assessed by simulating equiprobable DEMs directly from the original data (Goovaerts, 1997). The uncertainty about the value of a variable at a non-sampled point depends both on the spatial configuration and on the values of the surrounding sampling points. Classical statistics cannot address this problem because they do not account for the spatial data configuration. Simulation-based methods are consistent

with the concept of random variable, i.e. a variable that can take a series of outcome values according to some probability distribution. The local uncertainty is given by any statistical measure of dispersion from the set of realizations at a given location (point-to-point statistic). Spatial features are deemed certain if seen on most realizations, which expresses the spatial uncertainty (Goovaerts, 1997). Of the many simulation techniques available the sequential indicator simulation is appropriate for contour data because it allows: (1) the incorporation of secondary information including 'inequality data' (Deutsch and Journel, 1998) and, (2) the modeling of several indicator variograms for several cutoffs, which permits the reproduction of class-specific patterns. Inequality data are interval data of which we know only the boundaries. Contour elevation values may be considered as such boundaries for interpolated elevation data located between contour traces. Class-specific patterns of elevation on watersheds are common; lower elevation values are observed along river channels while higher elevation values are usually located along crest lines and towards summits.

2.3. Propagation of DEM uncertainty to slope models

Of the numerous DEM derivatives, the slope gradient has been one of the most studied. Indeed, the slope gradient controls the rate of surface and subsurface movement of material (soil, water, pollutants), hence its importance in a wide range of disciplines, including pedology, land evaluation, hydrology, civil engineering. Different slope algorithms have been proposed and compared for their accuracy (Evans, 1980; Zevenbergen and Thorne, 1987; Eyton, 1991; Florinsky, 1998; Jones, 1998; Corripio, 2003; Warren et al., 2004). They can be classified in three groups, depending on whether the slope gradient is approximated using (1) trigonometry or (2) differential geometry (Warren et al., 2004), or (3) vectorial algebra (Corripio, 2003). The trigonometric approach, also referred to as the 'Maximum Downward Gradient' (MDG) computes the slope gradient as a change in elevation over a certain distance; the elevation at a point is compared with the elevations of its eight neighbors, and the largest slope gradient of the corresponding eight slope gradients is adopted. This approach is seldom used, because it considers only eight possible directions of steepest slope. The approach based on differential geometry is the commonly used and consists in two operations:

(1) Fitting a differentiable, bivariate function to the elevation z in a DEM moving window:

$$z = f(x,y) \tag{4}$$

where x and y are plan Cartesian coordinates,

(2) Computing the slope gradient as a magnitude of the gradient vector (tangent vector of the surface pointing in the direction of steepest slope; Warren et al., 2004):

$$\text{slope gradient} = \sqrt{f_x^2 + f_y^2} \tag{5}$$

where f_x and f_y are partial derivatives of the bivariate function. The often-used slope algorithms are of two types, depending on whether the partial derivatives f_x and f_y are approximated using the four or eight closest pixels in a three by three DEM window (Burrough and McDonnell, 1998). They will be referred to as 4-neighbor and 8-neighbor henceforth.

The method based on vectorial algebra calculates the slope gradient using the smallest surface unit of the DEM (Corripio, 2003). As such, this method minimizes the smoothing effect that characterizes methods based on differential geometry.

In many applications, the slope gradient, like other DEM derivatives, is used as a predictor or explanatory variable for another target variable. In this case, one is more concerned about the uncertainty rather than the accuracy of the predictor's value. Therefore, in this study the performance comparison of slope algorithms will be based on their sensitivity to DEM uncertainty. Previous studies on DEM uncertainty propagation indicate that slope models utilizing more neighboring pixels or larger moving windows are less sensitive to DEM uncertainty (Albani et al., 2004; Raaflaub and Collins, 2006). This implies, a priori, that the 4-neighbor models are more sensitive to DEM uncertainty than the 8-neighbor models. However, some GIS software use the 4-neighbor slope models in developing other useful topographic models, like the wetness index (Beven and Kirkby, 1979). For example, LandMapR (MacMillan, 2003) uses a 4-neighbor slope algorithm (the Eyton's algorithm; Eyton, 1991) to compute the wetness index and for a fuzzy-based landform classification. In this case, it would be desirable to check whether difference in the DEM uncertainty propagation between the 4- and the 8-neighbor models is significant, which would justify changing the formula for the wetness index or any other slope-based variable. Two representatives of such slope algorithms will be considered here: the Zevenbergen and Thorne method (4-neighbor method) and the Evans–Young method (8-neighbor method).

Let S be the slope gradient (%) at a location with elevation z_5, surrounded by eight elevation data, z_1 to z_4 and z_6 to z_9 with a numbering as shown in Fig. 1, and w being the DEM resolution.

The Zevenbergen and Thorne algorithm (Zevenbergen and Thorne, 1987) is based on the 4 cardinal neighboring points:

$$S = \sqrt{\left(\frac{z_6 - z_4}{2w}\right)^2 + \left(\frac{z_2 - z_8}{2w}\right)^2}. \tag{6}$$

The Evans–Young (Shary et al., 2002) algorithm uses all surrounding data:

$$S = \sqrt{\left(\frac{z_3 + z_6 + z_9 - z_1 - z_4 - z_7}{6w}\right)^2 + \left(\frac{z_1 + z_2 + z_3 - z_7 - z_8 - z_9}{6w}\right)^2}. \tag{7}$$

The two algorithms will be evaluated based on their relative sensitivity to DEM uncertainty propagation.

3. Materials and methods

3.1. Study area

The study area is an 8 km by 5.5 km area enclosing 2 contiguous watersheds in southern Burundi. Actually we were interested only in the two watersheds, but for DEM interpolation purposes it was necessary to select a rectangle enclosing the two watersheds. Therefore, only the zone corresponding to the two watersheds will be considered in the evaluation of the DEM interpolation methods and slope algorithms. This zone will be referred to as 'test site'. The only topographic information available was a 1:50 000-scale topographic map with 20-m contour interval. This is the most detailed topographic map available that covers the whole country. The contour values range from 1820 m to 2080 m. The study site belongs to the 'Central plateaus' region, which extends to more than half of the country and is dominated by a hilly landscape. Two perpendicular patterns are evident by contours and the river network: an E–W orientation corresponding to the orientation of the three main

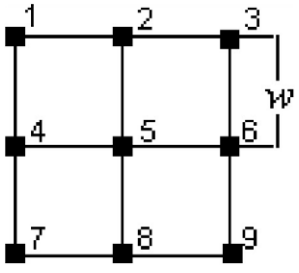

Fig. 1. Moving window definition for slope models.

rivers, two of which border the study area in the N and S; and an N–S orientation which corresponds to the direction of secondary river channels at their connection to the three main rivers. Isolated hills form an N–S alignment, which is also the general orientation of lithologic units in the case study. The study area is characterized by complex landscapes as suggested by the spacing between contours. The slope steepness is least (greatest contour spacing) around the main rivers and maximum (minimum contour spacing) towards the summits and the heads of the secondary river channels (Fig. 2).

3.2. DEM interpolation methods

First the minimum spacing between sampling points and the appropriate DEM resolution were selected. For the DEM resolution we applied the cartographic rule (Tempfli, 1999). The scale of the original topographic map was 1:50 000, so the optimal DEM resolution was fixed at 20 m and the minimum spacing between digitized contour nodes was set to 40 m (Smith and Wessel, 1990). The second step was selecting interpolation methods that allow extrapolation beyond the local minima and maxima. As already mentioned, preference was given to common GIS software. Surfer (Golden Software Inc., 2002) and Idrisi (Eastman, 2003) were used to select methods that allow extrapolation. Five of such methods were selected: (1) a method based on a triangulated irregular network (TIN) (we used the modules 'TIN' and 'TINSURF' implemented in Idrisi Kilimanjaro version (Eastman, 2003)), and four grid-based methods: (2) ordinary kriging, (3) minimum curvature (MC), (4) radial basis functions (RBF), and (5) the modified Shepard's method (MS) (for which we used Surfer v.8 (Golden Software Inc., 2002)). A detailed theoretical description of these methods is beyond the scope of this paper, so only a short description follows.

A TIN is built from joining known point values (contour vertices in our case) into a series of non-overlapping triangles based on the Delaunay triangulation (Burrough and McDonnell, 1998). In Idrisi Kilimanjaro, both points and contours may be used as input. However, TIN pre-processing is only possible when the input data are contours (Eastman, 2003). This consists of: (1) addition or deletion of extra vertices along contour lines, (2) constraining the triangulation to avoid triangle edges that cross contours, or (3) extrapolation beyond the data range by removal of so-called 'bridge and tunnel' (B/T) edges. A B/T edge is any triangle edge with end points that have the same value but are not neighboring points on a contour. As the names suggest, a 'bridge edge' is a triangle edge that lies above the true surface, while a 'tunnel edge' is a triangle edge that lies below the true surface. B/T edges likely occur near hill tops, valley bottoms, along ridges or channels, and along slopes where contours are undulating. These artifacts are corrected in Idrisi by: (1) adding new points (the so-called 'critical points') at midpoints of B/T edges, (2) adjusting the TIN and (3) interpolating the elevation at the new points. Interpolation is performed either by fitting a parabolic shape to surrounding contours (the recommended method) or by linear interpolation using a linear polynomial equation. The TIN model can be converted into a raster model using the 'TINSURF' Idrisi routine.

Kriging predicts a value at a non-sampled location by a weighted linear combination of values at surrounding locations. The weights depend on the data configuration and are obtained using a variogram model or structure, which expresses the spatial variability of the phenomenon under study. A variogram model is typically characterized by three parameters: (1) the nugget variance, which represents all sources of random noise (e.g. measurement or sampling errors) and variability at distances smaller than the sampling interval; (2) the range (i.e. range of correlation) which is the maximum distance of spatial correlation between observations of the investigated variable; and (3) the sill, which represents the total variance. The often-used variogram models are the linear, Gaussian, spherical and exponential models (Goovaerts, 1997).

The MC method generates the smoothest surface while attempting to honor sample data as closely as possible. The method consists in repeatedly applying a spline function over the grid until successive changes in the pixel values are less than a user-specified maximum residual value, or until a user-specified number of iterations is reached. Two parameters, i.e. the 'internal tension' and the 'boundary tension', control the bowing between samples and at the edges respectively (Smith and Wessel, 1990).

The MS method is an inverse-distance-least squares interpolator. As such, the method is similar to the inverse distance to a power method.

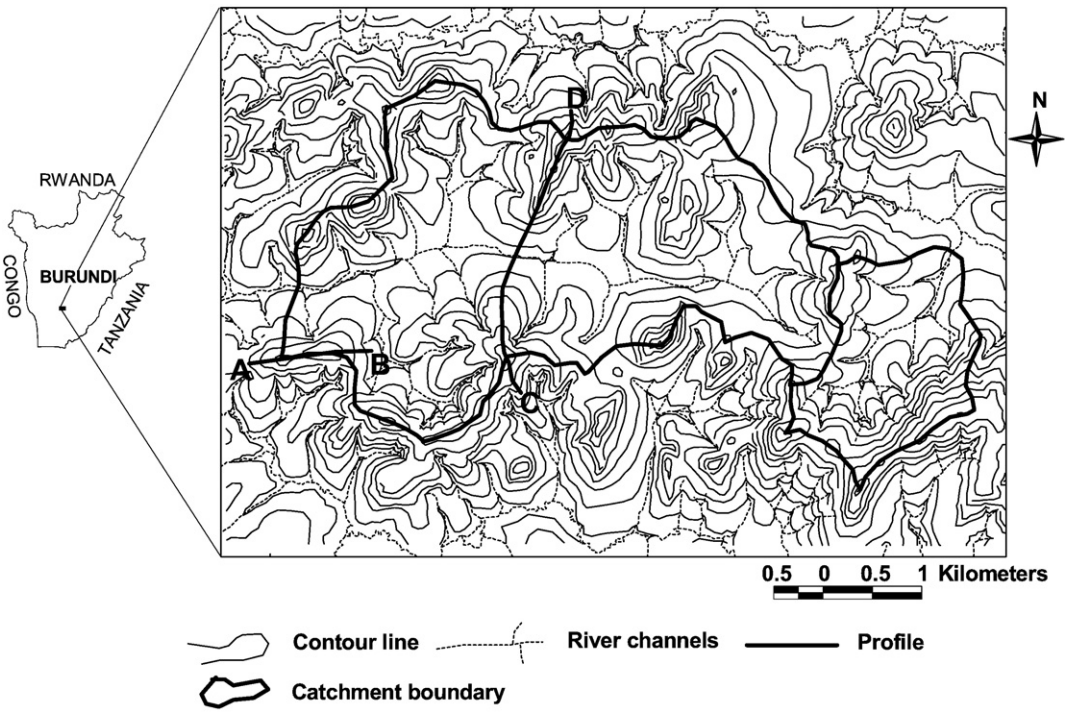

Fig. 2. Study area with contours, river channels, watersheds, profiles AB and CD.

However, the use of least squares in the MS method allows reducing the 'bull's eye' artifact that characterizes the inverse distance to a power method. The method starts by computing a local least squares fit of a quadratic surface around each observation. The number of local neighbors to use at this stage is given by the 'Quadratic Neighbors' parameter. The interpolated values are generated using a distance-weighted average of the previously computed quadratic fits at neighboring observations. The number of local neighbors for this operation is given by the 'Weighting Neighbors' parameter. For the two parameters, Surfer v.8 assigns default values following recommendations by Renka (1988).

The RBF method comprises a diverse group of interpolation methods (Carlson and Foley, 1991). The functions used are kernel basis functions that define the optimal weights to apply to the data points when interpolating a grid node. The multiquadratic basis function is usually recommended (e.g., Aguilar et al., 2005) and was used here.

In MS and RBF, the smoothness is controlled by so-called 'smoothing factor' and 'shape factor' respectively. Other optimization options include, accounting for anisotropy (kriging, MC, MS and RBF), and defining the search neighborhood (kriging, MS and RBF). It is also possible to incorporate 'breaklines' (kriging, MC, RBF) or 'faults' (kriging and MC). Breaklines are used to define discontinuities in the slope, while faults act as barriers to information flow; samples located on one side of a fault are not used during interpolation on the other side.

The TIN-based DEM was constructed from the original contours after having added extra nodes by setting a maximum spacing distance between nodes to 40 m. For the other methods (kriging, MC, MS and RBF), the original contour lines were generalized to contour nodes using also a tolerance distance of 40 m.

3.3. DEM uncertainty

The DEM uncertainty was modeled by sequential indicator simulation, using 'SISIM', a GSLIB routine (Goovaerts, 1997; Deutsch and Journel, 1998). The indicator approach requires selecting different thresholds from the cumulative distribution function (cdf) of the variable. However, the cdf of elevation obtained from contour nodes typically shows a step-like shape which is not representative of the real topography. Therefore the cdf was approximated from a sample of DEM pixel values. Elevation nodes from the DEM obtained using TINSURF were sampled using a tolerance distance of 40 m (i.e. 2 times the DEM resolution).

From the new elevation dataset up to 10 thresholds were selected and corresponding indicator values were calculated. Given a threshold $z_k \in]z_j, z_{j+20}[$, where z_j and z_{j+20} are elevation values in meters for two consecutive contour lines on a topographic map with 20-m contour interval, such that $z_{j+20}=z_j+20$ m, the indicator variable $i(\mathbf{u}; z_k)$ at a location $\mathbf{u}$ is:

$$i(\mathbf{u};z_k)=\begin{cases}1 & \text{if} \quad z\le z_j\\ \text{undefined for} & z\in]z_j, z_{j+20}[\\ 0 & \text{if} \quad z\ge z_{j+20}\end{cases}. \tag{8}$$

Interestingly, this way of coding allows obtaining more hard data values (0's and 1's) for modeling indicator variograms. Indeed, the undefined values in relation (8) become 1's when moving to thresholds higher than z_k. Still, relation (8) does not account for the implicit increase of elevation from z_j to z_{j+20} inside the constraint interval $]z_j, z_{j+20}[$. If $z\in]z_j, z_{j+20}[$, the probability for having z higher than threshold z_k decreases as z values get closer to z_j and increases as z values get closer to z_{j+20}. Therefore, relation (8) was replaced by relation (9):

$$i(\mathbf{u};z_k)=\begin{cases}1 & \text{if} \quad z\le z_j\\ \dfrac{z_{j+20}-z}{20} & \text{for} \quad z\in]z_j, z_{j+20}[\\ 0 & \text{if} \quad z\ge z_{j+20}\end{cases}. \tag{9}$$

This way, all the input data may be used for modeling the indicator variograms.

The program POSTSIM, also available in GSLIB (Deutsch and Journel, 1998) was used to compute the conditional variance as a measure of DEM uncertainty.

3.4. Performance comparison

The DEM interpolation methods were compared using both qualitative and quantitative criteria. Qualitative criteria were: (1) checking for artificial terraces using the script proposed by Hengl et al. (2003), (2) profiling, (3) watershed delineation, and (4) reconstruction of the drainage network from the interpolated DEMs by using the Idrisi routines 'PROFILE', 'WATERSHED' and 'RUNOFF', respectively. The ME and RMSE were combined to quantify the precision, using relation (3). For this, the interpolation dataset was split into a calibration dataset and a validation dataset. Since different interpolators usually perform similarly in zones of high sampling density, we compared the performance of the interpolators in a situation of lower sampling density. This situation was simulated by setting a tolerance distance of 100 m between the validation points and the calibration points. The validation dataset was composed of 184 points selected randomly from the original interpolation points and located in the test site. Because the validation points were taken from contour vertices whereas the TIN-based method is optimal when using contours, only qualitative criteria were applied to the TIN-based method.

Two slope algorithms were compared: the Zevenbergen and Thorne algorithm (ZT), which belongs to the 4-neighbor methods, and the Evans–Young algorithm (EY), which is an 8-neighbor method. The comparison criterion for the two algorithms was the sensitivity to DEM uncertainty propagation. From the simulated DEMs, slope gradient models were derived using each of the two algorithms, and their point-to-point variances were compared.

4. Results and discussion

4.1. Evaluation of DEM interpolation methods

TINSURF generated a DEM from a TIN obtained with the constrained triangulation option in the Delauney triangulation, and with the parabolic fit option for the B/T removal. For kriging, MC, MS and RBF, the options and parameters which were used are given in Table 1. MS produced exaggerated angular summits with the recommended values of the smoothing factor (between 0.0 and 1.0; see Golden Software Inc., 2002). Therefore the smoothing factor was increased to 2.0 to reduce these angularities.

Table 1
Options and parameters used in DEM interpolation by kriging, MC, MS and RBF

Interpolation method	Options and parameters
Kriging	Kriging type: point ordinary kriging. Variogram model: double spherical (nugget variance: 0 m^2; range: 750 m (first structure) and 1200 m (second structure); sill: 850 m^2 (first structure) and 750 m^2 (second structure)). Search radius: 4780 m (8 search sectors; 3 maximum data per sector; 5 maximum empty sectors; maximum 24 data in all sectors; minimum 8 data in all sectors).
MC	Maximum residual: 0.28 m; maximum iteration: 100,000; internal tension: 0; boundary tension: 0.
MS	Smoothing factor: 2; quadratic neighbors: 13; weighting neighbors: 19; search radius: 956 m.
RBF	Basis function: multiquadratic; shape factor: 720. Search radius: 4780 m (4 search sectors; 16 maximum data per sector; 3 maximum empty sectors; 8 minimum data in all sectors; 64 maximum data in all sectors).

Using the script proposed by Hengl et al. (2003), we checked for the presence of artificial terraces in the DEMs. No terrace was detected in DEMs produced with TINSURF, MC, MS and RBF, whereas one terrace was identified in the kriging-based DEM. In reality, flat areas exist, especially in the valley bottoms, but they are not documented on topographic maps, and their reproduction by an interpolator is likely to be an artifact rather than a performance. A precise delineation of valley bottoms is crucial in hydrological, ecological and agricultural applications, because bottom valleys and hillsides are characterized by fundamentally different soil and water dynamics. The only way to successfully delineate the two types of landscapes is the use of field measurements or high-resolution satellite or airborne imagery.

Fig. 3 shows the river channels and watersheds generated from the DEMs. These watersheds were automated by specifying outlet zones A and B (Fig. 3(a)) as seed images in the 'WATERSHED' Idrisi module. Notice that these outlet zones were set large enough and centered to the river channels that were digitized from the original topographic map. Therefore, failure to reproduce the delineation of watersheds was only due to limitations of the DEM interpolators. As a reference, the contours and drainage patterns that were digitized from the original topographic map were also given in Fig. 3(a). For performance comparison, the original contours were overlaid on the DEM-derived watersheds and river channels. The four encircled zones 1, 2, 3 and 4 on Fig. 3 were identified as problematic zones because the spacing between contours is larger than in the surrounding areas. Important deviations (>100 m) of DEM-derived river channels relative to those shown on the original topographic map were observed in zone 2 for kriging; in zones 1 and 2 for MC; in zones 1, 2 and 3 for MS; and in

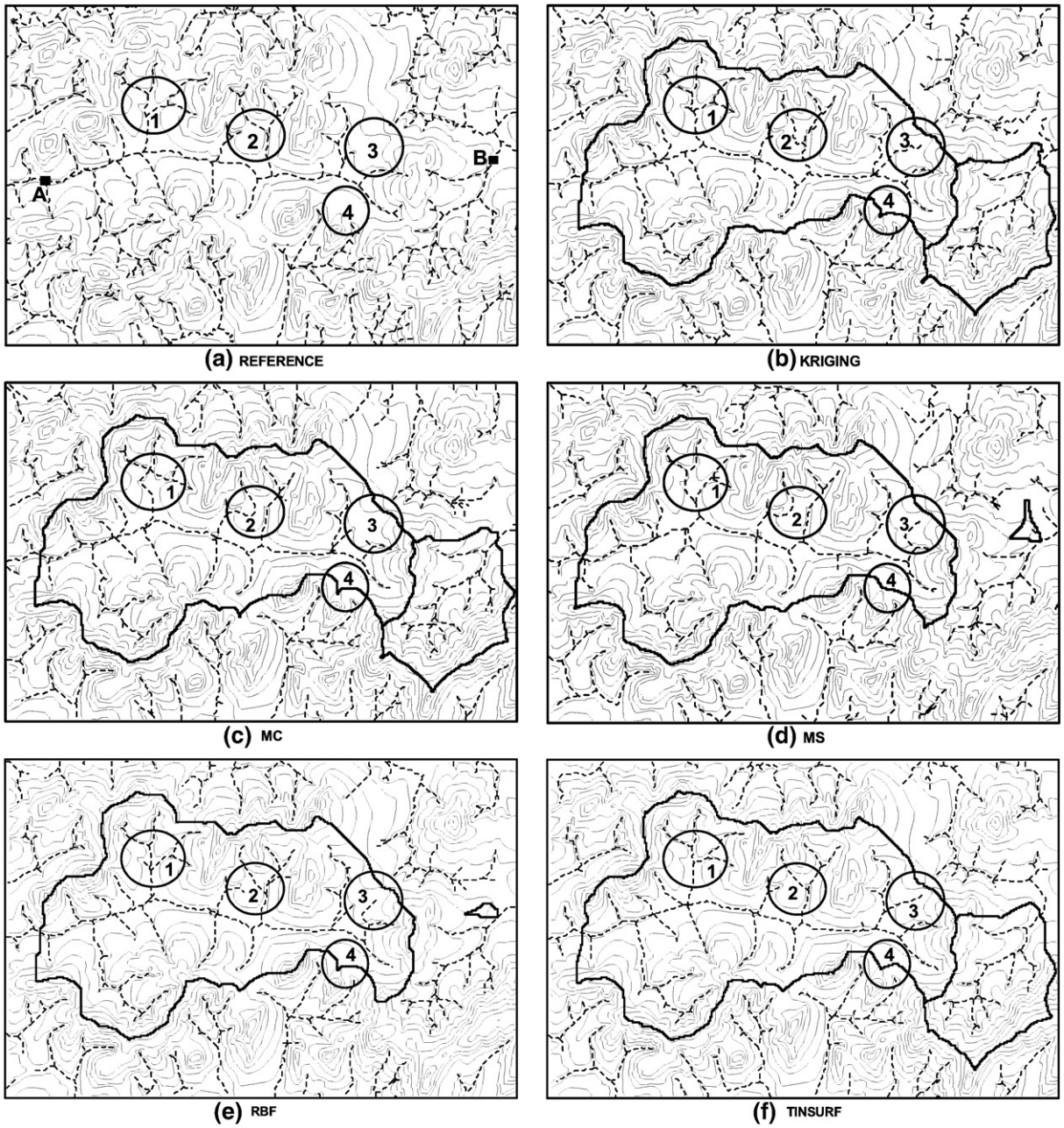

Fig. 3. River channels (dashed lines) and watersheds (thick lines) derived from DEMs obtained with different interpolation methods. Encircled areas are control zones, and the black squares A and B are the outlet zones of both watersheds. (a): Contours and river channels from the original topographic map; (b)–(f): DEM-derived watersheds and river channels using the five interpolation methods: (b) kriging; (c) MC; (d) MS; (e) RBF; (f) TINSURF. The original contours overlay the DEM-derived watersheds and river channels.

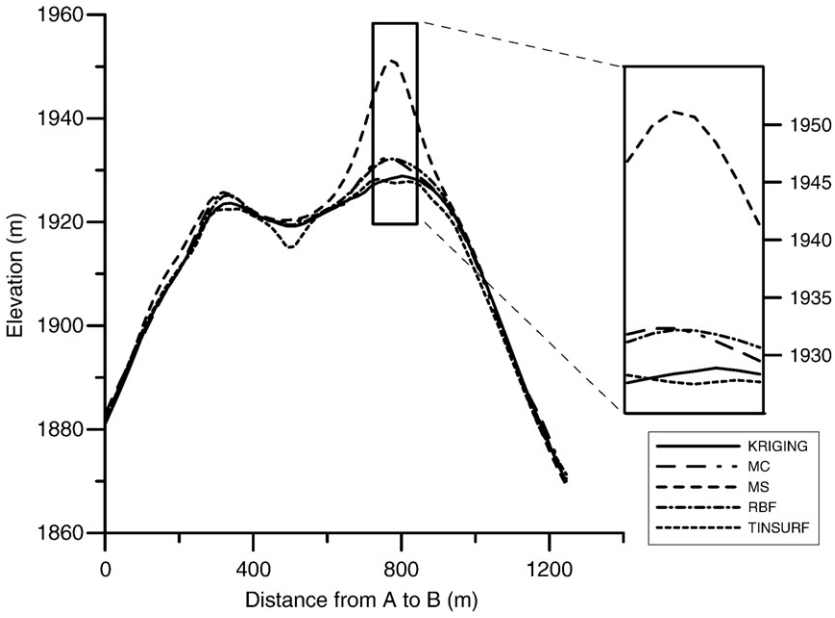

Fig. 4. DEM profiles along line AB (see Fig. 2). Kriging, MC, RBF and TINSURF give acceptable profiles, whereas MS over-estimates one summit beyond the allowable elevation range, which is in between 1820 m and 1840 m. The parameters and options used for Kriging, MC, MS and RBF are given in Table 1.

zone 3 for RBF. These important deviations were not observed for TINSURF. In general the watershed corresponding to outlet A was correctly delineated by all the five interpolators considered. Inside zone 4, the pattern of contours indicates a hill oriented N–S and having a summit at the southern limit of zone 4. Therefore the extent of the watershed should match a part of the hill. This was accomplished by kriging, MC, RBF and TINSURF, but not by MS. The watershed corresponding to outlet B was excessively under-estimated by MS and RBF. This was because the channels (dashed lines on Fig. 3) derived from those two interpolators did not intersect the outlet zone. Notice that similar problems would have been observed with kriging, MC and MS, but not with RBF, if we were to delineate smaller watersheds by choosing outlets in zone 2 where RBF reproduces the river channels better than kriging, MC and MS. From these results, a ranking of the methods in terms of watershed and channels delineation is:

$$\text{TINSURF} > \text{MC} = \text{kriging} = \text{RBF} > \text{MS}. \quad (10)$$

Fig. 4 shows DEM profiles along transect AB (see Fig. 2). The pattern of the original contours suggests that transect AB passes through two summits. Since the nearest contours for the two summits have the same value (1920 m), allowable values for the two summits must be higher than 1920 and lower than 1940. This condition was fulfilled by TINSURF, kriging, MC and RBF, but was violated by MS. For the TIN-based method, artificial abrupt changes could be expected due to the triangulation process (Burrough and McDonnell, 1998). So the performance of the methods in terms of interpolation of acceptable values and profiles can be ranked as:

$$\text{MC} = \text{kriging} = \text{RBF} > \text{TINSURF} > \text{MS}. \quad (11)$$

Table 2 gives the precision values that were obtained by comparing interpolated values with actual contour values at the 184 validation points. As mentioned already TINSURF was not used here since it performs better when applied to contours than to points. Considering the global precision values, i.e. computed using all the validation points (Table 2, last row), the relative performances were ranked as:

$$\text{MC} = \text{kriging} = \text{RBF} > \text{MS}. \quad (12)$$

When the precision values were considered for each contour value (Table 2), then the relative performances differed among contour values. In general, MS performed worst at most contour values but it gave better results at extreme contour values; it was the best at contour value 1860 m, and the second together with kriging at contour value 2060 m. Contrary to the MS, the difference in precision between kriging, MC and RBF was not pronounced; of the 10 contour values considered (Table 2), the largest difference in precision was 2 m. When accounting for these small differences, MC was ranked best and RBF was better than kriging.

Therefore, the general ranking related to the precision indices became:

$$\text{MC} > \text{RBF} > \text{kriging} > \text{MS}. \quad (13)$$

Kriging is a popular interpolation method, but, as the overview of the results in Table 2 indicates, MC and RBF were found to be superior to kriging in terms of local accuracy.

Table 2
Performance comparison between kriging, MC, MS and RBF, based on the precision index

Contour value (m)	N[a]	Precision (m)				Ranking
		Kriging	MC	MS	RBF	
1860	22	11	11	**9**	11	MS>kriging=MC=RBF
1880	30	10	**9**	13	**9**	MC=RBF>kriging>MS
1900	38	7	**6**	21	7	MC>kriging=RBF>MS
1920	32	**8**	**8**	15	**8**	kriging=MC=RBF>MS
1940	24	8	**7**	9	**7**	MC=RBF>kriging>MS
1960	16	8	**7**	11	**7**	MC=RBF>kriging>MS
1980	8	10	**7**	27	8	MC>RBF>kriging>MS
2000	5	6	**4**	21	**4**	MC=RBF>kriging>MS
2020	6	**7**	**7**	9	**7**	kriging=MC=RBF>MS
2060	3	11	**10**	11	12	MC>kriging=MS>RBF
All	184	**9**	**9**	16	**9**	kriging=MC=RBF>MS

The best precision for each contour value is in bold.
[a] N is the number of validation points.

It was concluded that none of the five interpolation methods was superior for all the validation criteria. However, MS was worst for all criteria. MC outperformed the other grid-based interpolation methods, but TINSURF was best in terms of correctness of channels delineation. However, TIN-based interpolation methods are known to produce DEMs with artificial triangular facets (Burrough and McDonnell, 1998). Therefore, MC and TINSURF were combined as follows:

(1) sampling the DEM from the TINSURF method with a 40 m tolerance distance,
(2) interpolating a DEM from the sampled points using MC.

The rationale behind this combination was correcting for the artificial triangular facets of the DEM from TINSURF using a smoothing interpolator. For the DEM obtained with the combined method, no artificial triangular facets were observed, and the reproduction of watersheds and river channels was as good as with TINSURF alone. In a similar manner, TINSURF was combined with the other grid-based methods (kriging, MS, RBF), and all the combinations gave satisfactory results. This is because the tolerance distance (40 m) that was used to sample the TIN-based DEM was kept short.

Fig. 5 represents the DEM obtained by combining MC and TINSURF (a), and the derived slope image using the EY algorithm (b). The crests and channels networks appear on the DEM as high and low grey levels, respectively. For the slope image, both the crests and channels networks appear in low grey levels, indicating minimum slope gradients. Maximum slope gradients (high grey levels) can be observed around the crests and at the heads of secondary river channels. All these observations from the DEM and slope image are in agreement with the pattern of the original contour lines (Fig. 2). Artificial terraces, which are often reported for slope maps obtained from contour-derived DEMs (e.g. Burrough and McDonnell, 1998), were not observed. Combinations of TINSURF with the other grid-based methods gave similar results as combination of TINSURF with MC.

4.2. DEM uncertainty and its propagation

Profiles from individual DEM realizations produced noisy representation of the elevation. While the real spatial variation of some environmental variables may be effectively noisy, this is usually not the case for topography. Therefore, the 100 DEM realizations were filtered as to approximate the smooth topography inferred from the original contours. A moving averaging filter using a three by three pixels window was passed over each DEM realization three times. At each pass, filtered DEM realizations were evaluated by deriving

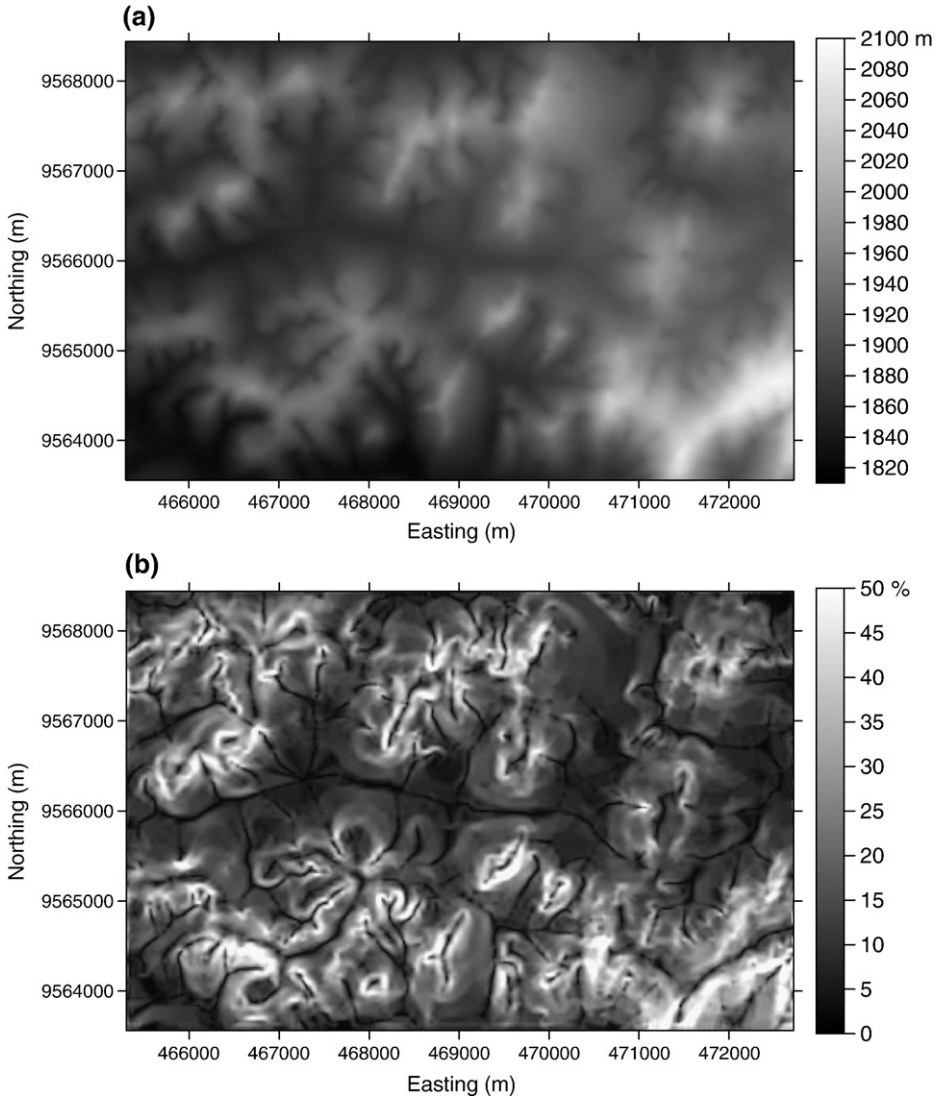

Fig. 5. DEM obtained by combining TINSURF and MC (a) and corresponding slope gradient map using the Evans–Young algorithm (b).

contour maps of 20-m contour interval (the same as the original contour map) and comparing these with the original contour map. Fig. 6 represents profiles of a DEM realization before and after applying such a filter. The unfiltered DEM profile shows only the long-range features of the hillslope, but the short-range variability is exaggerated. After filtering the local variation the DEM profile is much more continuous and realistic.

The filtered DEMs were subsequently used to derive slope gradients according to the EY and ZT slope algorithms. To assess the DEM and slope uncertainty, variances for the elevation and slope gradient were derived from the 100 DEMs and associated slope realizations, before and after filtering. The two slope algorithms were compared based on the slope variances. Let Var_{ZT} and Var_{EY} be the variances for the slope gradient when using the ZT and EY algorithms, respectively. The difference in slope variance between the 2 algorithms is:

$$\Delta Var_S = Var_{ZT} - Var_{EY}. \quad (14)$$

Positive variance differences would indicate that the ZT algorithm is more sensitive to DEM uncertainty than the EY method, and vice versa. It is worth noting that the variances were computed for each location (pixel) in the test site from the 100 simulated values, and are to be considered as a measure of local uncertainty. The number of pixels in the test site was 37,682.

Table 3 provides quantiles corresponding to the 5th, 50th and 95th percentiles; for the point-to-point statistics of: (1) the variances of the simulated DEMs, (2) Var_{ZT}, (3) Var_{EY} and (4) ΔVar_S, before DEM filtering and after DEM filtering.

In more than half of pixels in the test site, the variance of the raw elevation, i.e. before filtering, was less than 100 m^2. In 95% of pixels in the test site, the variance was less than 181 m^2, i.e. less than half of the allowable maximum uncertainty which is 400 m^2 (i.e. standard deviation < contour interval, which is 20 m in our case). Yet these figures are not providing a complete basis for evaluation since they correspond to simulated DEMs with exaggerated roughness, as shown on Fig. 6. After filtering, the variance of the elevation was less than

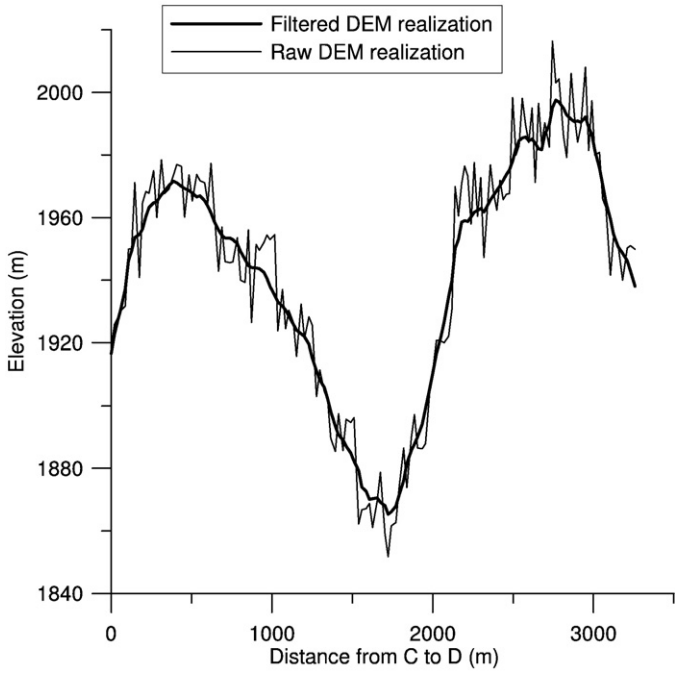

Fig. 6. Profiles along line CD (see Fig. 2) for a simulated DEM, before filtering (thin line) and after filtering (thick line).

Table 3
Quantiles of point-to-point simulated DEM variance, Var_{ZT}, Var_{EY} and ΔVar_S

	Before post-processing			After post-processing		
	5th	50th	95th	5th	50th	95th
	percentile			percentile		
DEM variance (m^2)	0	96	181	3	7	14
Var_{ZT} ($\%^2$)	208	557	1440	13	24	50
Var_{EY} ($\%^2$)	123	254	709	11	22	44
ΔVar_S ($\%^2$)	−8	297	831	1	2	6

14 m^2 in 95% of the pixels in the test site (i.e. standard deviation < 4 m). It must be stressed here that filtering was primarily applied so as to obtain realistic DEM realizations from which reliable variances for the test site could be derived. Variance values obtained from the raw DEM realizations and corresponding slopes would be applicable to extremely rough topography as suggested on Fig. 6. The difference in slope variance between the two slope algorithms, ΔVar_S, was positive in 94.7% of the pixels in the study site before filtering. Before filtering, the quantiles of variances for the two slope algorithms were extremely large, and the quantiles for Var_{ZT} were twice as large as those for Var_{EY}. In our test site, where the roughness was approximated by the filtered DEMs, the two slope algorithms may be used without significant differences; in 95% of the pixels in the test site, $\Delta Var_S < 6\%^2$.

5. Conclusion

In this study we tried to derive reliable topographic models from contours. Special attention was paid to the reproduction of the terrain shape, which is more important than absolute accuracy in many environmental applications.

For DEM interpolation, only interpolators that allow extrapolation to local minima and maxima – which were not explicitly documented on contour maps – were selected. In this respect, a TIN-based method and four grid-based interpolators (kriging, minimum curvature, modified Shepard's method and radial basis function) proved successful, while avoiding artificial terraces which are common artifacts in contour-derived DEMs. The reproduction of channel networks and watersheds was worse with the modified Shepard's method but excellent with the TIN-based method. However, TIN-based methods are known to produce artificial sharp triangular edges. These could be removed by combining the TIN-based method with kriging, MC, MS or RBF. Therefore, we recommend combining the TIN-based method with a grid-based interpolation method that is able to extrapolate outside the local data range.

Uncertainty assessment using indicator simulation and treating contour lines as constraint intervals, proved successful. However, although the simulated elevation uncertainty was within the allowable range (i.e. variance of less than 400 m^2 or standard deviation of less than 20 m), the simulated DEMs were too noisy compared to the real topography in the test site. Filtering the simulated DEMs resulted in realistic DEM realizations. The EY method was less sensitive to DEM uncertainty than the ZT method, but, after filtering, the difference between the two slope algorithms was not significant. Therefore, we concluded that both the two slope algorithms were appropriate. Overall, it was shown in this study that reliable topographic models can be derived from contours.

Acknowledgements

This research was financially supported by the Flemish Inter-university Council (VLIR). Digital copies of topographic maps we used for digitizing contours were kindly provided by the staff of the Royal Museum for Central Africa, Tervuren (Belgium).

References

Aguilar, F.J., Agüera, F., Aguilar, M.A., Carvajal, F., 2005. Effects of terrain morphology, sampling density, and interpolation methods on grid DEM accuracy. Photogrammetric Engineering & Remote Sensing 71, 805–816.

Albani, M., Klinkenberg, B., Andison, D.W., Kimmins, J.P., 2004. The choice of window size in approximating topographic surfaces from digital elevation models. International Journal of Geographical information Science 18, 577–593.

Beven, K.J., Kirkby, M.J., 1979. A physically-based, variable contributing area model of basin hydrology. Hydrological Science Bulletin 24, 1–10.

Biesemans, J., Van Meirvenne, M., Gabriels, D., 2000. Extending the RUSLE with the Monte Carlo error propagation technique to predict long-term average off-site sediment accumulation. Journal of Soil and Water Conservation 55, 35–42.

Burrough, P.A., McDonnell, R.A., 1998. Principles of Geographical Information Systems. Oxford University Press, New York, p. 333.

Carlson, R.E., Foley, T.A., 1991. Radial Basis Interpolation Methods on Track Data. Lawrence Livermore National Laboratory. UCRL-JC-1074238.

Carrara, A., Bitelli, G., Carla, R., 1997. Comparison of techniques for generating digital terrain models from contour lines. International Journal of Geographical Information Science 11, 451–473.

Corripio, J.G., 2003. Vectorial algebra algorithms for calculating terrain parameters from DEMs and solar radiation modeling in mountainous terrain. International Journal of Geographical Information Science 17, 1–23.

Desmet, P.J., 1997. Effects of interpolation errors on the analysis of DEMs. Earth Surface Processes and Landforms 22, 563–580.

Deutsch, C., Journel, A., 1998. GSLIB. Geostatistical Software Library and User's Guide. Oxford University Press, New York, p. 369.

Eastman, J.R., 2003. Idrisi Kilimanjaro. Guide to GIS and Image Processing. Clark Labs, Clark University, p. 328.

Evans, L.S., 1980. An integrated system of terrain analysis for slope mapping. Zeitschrift fur Geomorphologie 36, 274–295.

Eyton, J.R., 1991. Rate-of-change maps. Cartography and Geographic Information Systems 18, 87–103.

Fisher, P.F., 1998. Improved modeling of elevation error in geostatistics. GeoInformatica 2, 215–233.

Fisher, P.F., Tate, N.J., 2006. Causes and consequences of error in digital elevation models. Progress in Physical Geography 30, 467–489.

Florinsky, I.V., 1998. Accuracy of local topographic variables derived from digital elevation models. International Journal of Geographical Information Science 12, 47–61.

Florinsky, I.V., Kuryakova, G.A., 2000. Determination of grid size for digital terrain modeling in landscape investigation — exemplified by soil moisture distribution at a micro-scale. International Journal of Geographical Information Science 14, 815–832.

Golden Software Inc., 2002. Surfer 8.

Goovaerts, P., 1997. Geostatistics for Natural Resources Evaluation. Oxford University Press, New York, p. 483.

Hengl, T., 2006. Finding the right pixel size. Computers & Geosciences 32, 1283–1298.

Hengl, T., Gruber, S., Shrestha, D., 2003. Digital Terrain Analysis in ILWIS. Lecture notes, international Institute for Geo-information Science and Earth Observation (ITC), Enschede, p. 56.

Heuvelink, G., 1998. Error Propagation in Environmental Modeling with GIS. Taylor and Francis, London, p. 249.

Holmes, K.W., Chadwick, O.A., Kyriakidis, P.C., 2000. Error in a USGS 30-meter digital elevation model and its impact on terrain modeling. Journal of Hydrology 233, 154–173.

Hutchinson, M.F., 1996. A locally adaptive approach to the interpolation of digital elevation models. In: NCGIA (Ed.), Proceedings of the Third International Conference Integrating GIS and Environmental Modeling, 21–26 January 1996, Santa Fe, New Mexico.

Jaakkola, O., Oksanen, J., 2000. Creating DEMs from contour lines: interpolation techniques which save terrain morphology. GIM International 14, 46–49.

Jones, K.H., 1998. A comparison of two approaches to ranking algorithms used to compute hill slopes. GeoInformatica 2, 235–256.

Kidner, D.B., 2003. Higher-order interpolation of regular grid digital elevation models. International Journal of Remote Sensing 24, 2981–2987.

MacMillan, R.A., 2003. LandMapR© Software Toolkit-C++ Version: Users manual. LandMapper Environmental Solutions Inc., Edmonton, AB, p. 110.

Raaflaub, L.D., Collins, M.J., 2006. The effect of error in gridded digital elevation models on the estimation of topographic parameters. Environmental Modeling & Software 21, 710–732.

Renka, R.J., 1988. Multivariate interpolation of large sets of scattered data. ACM Transaction on Mathematical Software 14, 139–148.

Shary, P.A., Sharaya, L.S., Mitusov, A.V., 2002. Fundamental quantitative methods of land surface analysis. Geoderma 107, 1–32.

Smith, W.H.F., Wessel, P., 1990. Gridding with continuous curvature splines in tension. Geophysics 55, 293–305.

Tempfli, K., 1999. DTM accuracy assessment. Proceedings of the 1999 ASPRS Annual Conference, 17–21 May 1999, Portland, Oregon, pp. 1–11.

Warren, S.D., Hohmann, M.G., Auerswald, K., Mitasova, H., 2004. An evaluation of methods to determine slope using digital elevation data. Catena 58, 215–233.

Wilson, J.P., Gallant, C., 2000. Terrain Analysis: Principles and Applications. John Willey & Sons, New York, p. 512.

Wise, S., 2000. Assessing the quality for hydrological applications of digital elevation models derived from contours. Hydrological Processes 14, 1909–1929.

Wood, J., 1996. The Geomorphological Characterisation of Digital Elevation Models. PhD Thesis, Department of Geography, University of Leicester, UK.

Zevenbergen, L.W., Thorne, C.R., 1987. Quantitative analysis of land surface topography. Earth Surface Processes and Landforms 12, 47–56.